Pattern Recognition Letters 34 (2013) 655–662

Contents lists available at SciVerse ScienceDirect

Pattern Recognition Letters

journal homepage: www.elsevier.com/locate/patrec

Active contour model driven by local histogram fitting energy

Weiping Liu [a,b,*], Yanfeng Shang [c], Xin Yang [a]

[a] Institute of Image Processing and Pattern Recognition, Shanghai Jiao Tong University, Shanghai 200240, China
[b] Philips Research China, Shanghai 200233, China
[c] The Third Research Institute of Ministry of Public Security, Shanghai 201204, China

ARTICLE INFO

Article history:
Received 9 April 2012
Available online 23 January 2013

Communicated by G. Borgefors

Keywords:
Active contour model
Histogram distance
Image segmentation
Local fitting, Nonparametric

ABSTRACT

A nonparametric local region-based active contour driven by a local histogram fitting energy is presented. The energy is defined in terms of an evolving curve and two fitting histograms that approximate the distribution of object and background locally through a truncated Gaussian kernel. The kernel width for computing the fitting histograms should be different on different pixels, since the same kernel width applied may cause local minima of the energy. Three inequalities are introduced to determine whether larger kernel width should be considered. We do not assume any distributions in the presented method. The method therefore belongs to a nonparametric local region based active contour, and it can segment the regions whose distribution is hard to be predefined. Experimental results show desirable performances of our method.

1. Introduction

Active contour model (ACM) (Kass et al., 1988) is a very popular image segmentation technique, and has been widely utilized in many applications in computer vision. The basic idea is to evolve a closed curve so as to minimize a given energy functional. The evolving curve will stop when the energy functional reaches its minimum through gradient descent method. ACM can be categorized to two major classes: edge-driven and region-driven according to the type of extracted image features.

Edge-driven ACM utilizes image gradient to attract the evolving curve toward the boundary of desired object (Melonakos et al., 2008; Kass et al., 1988; Paragios et al., 2004; Caselles et al., 1997). These methods can locally stop the evolution when the evolving curve reaches a high gradient. However, their resistance to noise is still quite limited. A constant flow is added to edge-driven ACM in order to enlarge the capture range, but it is hard to choose an appropriate one, since either too large or too small one applied will cause undesirable segmentation result.

Region-driven ACM utilize more global information for segmentation due to different statistics of intensity or texture in the regions. Therefore, these methods are robust to noise and furthermore able to segment objects with weak boundary or even without edge. It is very important to model the distribution of the object and background in a region-driven ACM. Generally speaking, region-driven ACM can be further categorized to parametric and nonparametric methods, which is based on whether a predefined distribution is applied to estimate the intensity of the regions.

Gaussian and Gaussian Mixture distribution are popular models applied in parametric region-driven ACM. Chan–Vese model (C–V) (Chan and Vese, 2001) is based on the assumption of object and background intensity homogeneous. In fact, the probability density functions in C–V are Gaussian distribution with different means but same variance. In (Rousson and Deriche, 2002; Shang et al., 2008), the authors assume the distributions of each regions are Gaussian with means and variances undetermined. Shang (Shang et al., 2010) model regions by Gaussian Mixture model with several means and variances of Gaussian distribution to segment abdomen CT image. Although, the parametric region-based ACM can be applied in a variant of applications, such as medical image analysis (Shang et al., 2008) and aerial image partitioning (Cao et al., 2008), the object and the background in many images are hard to be described by a predefined distribution.

Nonparametric region-driven ACM does not suffer from the above limitation, since the distributions of different regions are estimated by a nonparametric statistical method. In (Jehan-Besson et al., 2003), the method is to minimize chi-2 distance function between a reference histogram of the region in previous image and a current estimated histogram for object tracking. In (Freedman and Zhang, 2004), Kullback–Leibler distance and Bhattacharyya distance for tracking distribution is presented, and the method is successfully applied to prostate segmentation in CT image which the grey level of the prostate is very similar in intensity with the soft tissues around it (Freedman et al., 2005).

* Corresponding author at: Institute of Image Processing and Pattern Recognition, Shanghai Jiao Tong University, Shanghai 200240, China. Tel.: +86 21 13816558743; fax: +86 21 54452890.
E-mail addresses: 6weiping@gmail.com (W. Liu), aysyf@126.com (Y. Shang), yangxin@sjtu.edu.cn (X. Yang).

0167-8655/$ - see front matter © 2013 Elsevier B.V. All rights reserved.
http://dx.doi.org/10.1016/j.patrec.2013.01.005

In (Kim et al., 2005), the authors present to maximize mutual information between the region labels and the image pixel intensities, namely minimize the conditional entropy which is represented by the probability density functions of each region approximated by Kernel Density Estimation. A histogram-based appearance model is present to segment kidney in CT image (Broadhurst et al., 2006), which Principle Component Analysis is utilized to learn appearance model from histograms computed from a set of learning sequence. Wasserstein distance using accumulative distribution function is introduced to histogram-based ACM (Chan et al., 2007), which claims the method outperforms the one that is pointwise with respect to histogram bins. In (Ni et al., 2009), a local histogram based active contour model using Wasserstein distance is presented. They compute the local histogram of the pixel in a patch, and then decide whether the pixel belongs to the inside region or outside region through computing the Wasserstein distance of the local histogram and the histogram inside and outside the closed curve. Although the method uses the local histograms, the histogram inside and outside the closed evolving curve are still computed globally. In (Chen and Radke, 2009), Kernel Density Estimation is applied to estimate the distribution of the histogram of rectum and background from a series of abdomen CT image, then they combine the learned histogram feature with a statistical shape model to evolve the active contour model.

Region-driven ACM can get more robust and global segmentation results, but most of the time the object is distinguished by local variations. Thus, a compromise between global and local feature is needed. Some researchers attempt to join edge and region-driven ACM (Chakraborty et al., 1996; Paragios and Deriche, 2002; Xie and Mirmehdi, 2004). However, the region and edge feature may not locally correspond (Xie and Mirmehdi, 2008), and there is no guideline to tell how to balance the local (usually edge feature) and global (usually region feature) feature. More recently, local region-driven ACM have been presented (Li et al., 2008; Zhang et al., 2010a; Wang et al., 2009; Lankton and Tannenbaum, 2008; Luo and Wu, 2011). The basic idea is to construct a local fitting energy in a local region confined by a kernel function. When a large kernel width is chosen, the model performs like a region-driven active contour model; when a small kernel width is chosen, the model performs like an edge-driven one. Thus, if an appropriate kernel width is chosen, the model can integrate the merits of edge and region-driven ACM. These methods achieve good performance on intensity inhomogeneity image which is hard to segment correctly using C–V model or piecewise smooth case of Mumford–Shah model (Tsai et al., 2001; Vese and Chan, 2002). However, these models lead to new drawbacks such as global coherence and homogeneous area problems (Piovano and Papadopoulo, 2008). The main reason of these new emerging problems is that there is no guideline to address the size of the kernel width.

In this paper, a nonparametric local region-based ACM driven by local histogram fitting energy is introduced. There are two main contributions. Firstly, local histogram fitting energy functional is introduced. The optimization of our method can drive the evolving curve according to local nonparametric statistical information represented by histogram. Secondly, three distances are defined to decide whether the current kernel width is appropriate. If any of the three distances is satisfied, the kernel width would be enlarged. Thus, different kernel width for computing the fitting histograms is utilized at different pixels.

The rest of the paper is organized as follows. Section 2 introduces local histogram based ACM. Section 3 presents our method. Firstly, a local histogram fitting energy is presented. Then three distances is defined to decide whether the kernel width is appropriate. At last, the paper gives the detail implementation using fast level set method and a technique to reduce the number of histogram bins to speed up the computation. The experiments in Section 4 demonstrate our method, and Section 5 concludes the paper.

2. Background and problem statement

A nonparametric region-driven ACM has been presented in (Ni et al., 2009; Chan et al., 2007). Let Ω is the image domain. A given grey image $I(\mathbf{x}) : \Omega \to [0, L]$ with two regions is isolated by a closed curve $\vec{C}$. $\vec{C}$ is able to evolve toward the ideal boundary of segmented objects. Denote the region inside and outside the curve $\vec{C}$ by Σ and Σ^c respectively. Let $N_r^{\mathbf{x}}$ be the local patch centered at $\mathbf{x}$ with radius r (patch scale). Define the local histogram and cumulative distribution function of a pixel $\mathbf{x} \in \Omega$ by

$$P_r^{\mathbf{x}}(z) = \frac{|\{y \in N_r^{\mathbf{x}} \cap \Omega : I(y) = z\}|}{|N_r^{\mathbf{x}} \cap \Omega|} \tag{1}$$

$$F_r^{\mathbf{x}}(z) = \frac{|\{y \in N_r^{\mathbf{x}} \cap \Omega : I(y) \leqslant z\}|}{|N_r^{\mathbf{x}} \cap \Omega|} \tag{2}$$

The energy functional of the local histogram based ACM takes the regional integral of histogram distances between the local histogram and the histogram of objects and background. The energy function is defined as (Ni et al., 2009)

$$E(\vec{C}, P_o, P_i) = \text{Length}(\vec{C}) + \lambda \int_{\Sigma} D(P_i, P_r^{\mathbf{x}}) d\mathbf{x} + \lambda \int_{\Sigma^c} D(P_o, P_r^{\mathbf{x}}) d\mathbf{x} \tag{3}$$

where P_i and P_o are two constant histogram inside and outside the evolving curve $\vec{C}$, respectively. λ is a constant parameter. $D(,)$ is a histogram distance. There are several kinds of histogram distance defined by different measure (Ma et al., 2010). Assume two histograms h and g with bin index $z \in [0, R]$. The common definition of histogram distances which have been used in some scientific literature are listed below:

$$D_{L_1}(h, g) = \int_0^R |h(z) - g(z)| dz \tag{4}$$

$$D_{L_2}(h, g) = \left(\int_0^R |h(z) - g(z)|^2 dz \right)^{1/2} \tag{5}$$

$$D_{\chi^2}(h, g) = \int_0^R \frac{|h(z) - g(z)|^2}{2(h(z) + g(z))} dz \tag{6}$$

$$D_{\text{KL}}(h, g) = \int_0^R h(z) \log \frac{h(z)}{g(z)} + g(z) \log \frac{g(z)}{h(z)} dz \tag{7}$$

$$D_B(h, g) = \int_0^R \sqrt{h(z) g(z)} dz \tag{8}$$

$$D_{W_1}(h, g) = \int_0^R \left| \int_0^z h(n) dn - \int_0^z g(n) dn \right| dz \tag{9}$$

They are L_1 distance, L_2 distance, Chi-2 distance (Jehan-Besson et al., 2003), Kull-back Leibler distance (Freedman and Zhang, 2004; Freedman et al., 2005), Bhattacharyya distance (Freedman and Zhang, 2004) and Wasserstein distance (Ni et al., 2009; Chan et al., 2007) from (4)–(9). These distance measures are defined by different theories and individual characteristics. The histogram distance $D(,)$ in (3) can be chosen from any of the distance listed above.

The energy functional in (3) can be represented in terms of level set method (Osher and Fedkiw, 2003) as follows:

$$E(\phi, P_o, P_i) = \int_\Omega |\nabla H(\phi(\mathbf{x}))| d\mathbf{x} + \lambda \int_\Omega H(\phi(\mathbf{x})) D(P_i, P_r^{\mathbf{x}}) d\mathbf{x} + \lambda \int_\Omega (1 - H(\phi(\mathbf{x}))) D(P_o, P_r^{\mathbf{x}}) d\mathbf{x} \quad (10)$$

where $H(\cdot)$ and ϕ are the Heaviside function and the level set function, respectively.

The curve evolution function is obtained by first choosing Wasserstein distance and then minimizing the above energy functional by variational and gradient descent method. The obtained curve evolution function are shown as follows: (Ni et al., 2009; Chan et al., 2007)

$$F_i(z) = \frac{\int_\Omega H(\phi(\mathbf{x})) F_r^{\mathbf{x}}(z) d\mathbf{x}}{\int_\Omega H(\phi(\mathbf{x})) d\mathbf{x}} \quad (11)$$

$$F_o(z) = \frac{\int_\Omega [1 - H(\phi(\mathbf{x}))] F_r^{\mathbf{x}}(z) d\mathbf{x}}{\int_\Omega 1 - H(\phi(\mathbf{x})) d\mathbf{x}} \quad (12)$$

$$\frac{\partial \phi}{\partial t} = \delta(\phi) \left[\nabla \cdot \left(\frac{\nabla \phi}{|\nabla \phi|} \right) - \lambda \int_0^R (|F_i(z) - F_r^{\mathbf{x}}(z)| - |F_o(z) - F_r^{\mathbf{x}}(z)|) dz \right] \quad (13)$$

where $\delta(\cdot)$ is Dirac function.

If L_1 distance is utilized, we get

$$P_i(z) = \frac{\int_\Omega H(\phi(\mathbf{x})) P_r^{\mathbf{x}}(z) d\mathbf{x}}{\int_\Omega H(\phi(\mathbf{x})) d\mathbf{x}} \quad (14)$$

$$P_o(z) = \frac{\int_\Omega [1 - H(\phi(\mathbf{x}))] P_r^{\mathbf{x}}(z) d\mathbf{x}}{\int_\Omega 1 - H(\phi(\mathbf{x})) d\mathbf{x}} \quad (15)$$

$$\frac{\partial \phi}{\partial t} = \delta(\phi) \left[\nabla \cdot \left(\frac{\nabla \phi}{|\nabla \phi|} \right) - \lambda \int_0^R (|P_i(z) - P_r^{\mathbf{x}}(z)| - |P_o(z) - P_r^{\mathbf{x}}(z)|) dz \right] \quad (16)$$

Our purpose of this study is illustrated in Fig. 1. Although the method of local histogram based ACM apply local histogram of the current pixels, the histogram of object and background are computed in global domain, see (11), (12), (14), and (15). Thus, if there are some background pixels that the local histogram of them are more similar to the object than the background, for example the mound in Fig. 1(a) and (b), the segmentation results will be fault, since it is inappropriate to decide the curve evolution by measuring the distance of the local histogram and the global mean histogram in this experiment. If the scale of local statistics is enlarged by increasing r, the problem still exists in Fig. 1(c) and (d). Moreover, the real boundary of the object is not accurate in Fig. 1(c) and (d). The only need is to model the background and object locally. It is difficult to say which segmentation result is better in Fig. 1(a) and (b) using L_1 distance and Wasserstein distance respectively. We believe there is no method superior to other one under any circumstances. Therefore, only L_1 distance is applied to illustrate our idea in this study. There is literature on how to decide the patch scale r adaptively (Hong et al., 2008), but this is not our focus. Instead, a fixed patch scale r is set to 3.

3. Proposed method

3.1. Local histogram fitting energy

In this section, a nonparametric region-driven ACM using local histogram fitting energy is presented. For a given point $\mathbf{x} \in \Omega$, the region is localized by a Gaussian kernel. The local histogram fitting energy is defined as follows:

$$E_{\mathbf{x}}^{LHF}(\bar{C}, P_i^{\mathbf{x}}, P_o^{\mathbf{x}}) = \int_\Sigma K_\sigma(\mathbf{x} - \mathbf{y}) D_{L_1}(P_i^{\mathbf{x}}, P_r^{\mathbf{y}}) d\mathbf{y} + \int_{\Sigma^c} K_\sigma(\mathbf{x} - \mathbf{y}) D_{L_1}(P_o^{\mathbf{x}}, P_r^{\mathbf{y}}) d\mathbf{y} \quad (17)$$

where $P_i^{\mathbf{x}}$ and $P_o^{\mathbf{x}}$ are the fitting histograms that approximate the distribution inside and outside the evolving curve $\bar{C}$ in position $\mathbf{x}$, respectively. $K_\sigma(\mathbf{x} - \mathbf{y})$ is a Gaussian kernel with variance $\sigma > 0$. It is represented by a truncated one as follows:

$$K_\sigma(\mathbf{d}) = \begin{cases} c \exp\left(-\frac{|\mathbf{d}|^2}{2\sigma^2}\right) & \text{if } |\mathbf{d}| \leqslant \rho \\ 0 & \text{if } |\mathbf{d}| > \rho \end{cases}$$

where c is a normalizing constant. ρ is the kernel width which defines the size of Gaussian mask, usually ρ is set to 2σ. The Gaussian mask can be computed by the method introduced in (Jain et al., 1995).

The local histogram fitting energy is a weighted distance of the local histogram $P_r^{\mathbf{y}}$ to the fitting histogram $P_i^{\mathbf{x}}$ and $P_o^{\mathbf{x}}$ with $K_\sigma(\mathbf{x} - \mathbf{y})$ as the weight assigned to each local histogram $P_r^{\mathbf{y}}$ at $\mathbf{y}$. The weights are dominated by the distance between $\mathbf{x}$ and $\mathbf{y}$. The local histogram fitting energy can be formulated in terms of the level set form as follows:

$$E_{\mathbf{x}}^{LHF}(\phi, P_i^{\mathbf{x}}, P_o^{\mathbf{x}}) = \int_\Omega H(\phi) K_\sigma(\mathbf{x} - \mathbf{y}) \int_0^R |P_i^{\mathbf{x}}(z) - P_r^{\mathbf{y}}(z)| dz d\mathbf{y} + \int_\Omega (1 - H(\phi)) K_\sigma(\mathbf{x} - \mathbf{y}) \int_0^R |P_o^{\mathbf{x}}(z) - P_r^{\mathbf{y}}(z)| dz d\mathbf{y} \quad (18)$$

Our ultimate goal is to minimize the local histogram fitting energy for all of the points in the whole image domain. Thus, the total energy is defined by:

$$\begin{aligned} E(\phi, P_i^{\mathbf{x}}, P_o^{\mathbf{x}}) &= \int_\Omega |\nabla H(\phi(\mathbf{x}))| d\mathbf{x} + \lambda \int_\Omega E_{\mathbf{x}}^{LHF}(\phi, P_i^{\mathbf{x}}, P_o^{\mathbf{x}}) d\mathbf{x} \\ &= \int_\Omega |\nabla H(\phi(\mathbf{x}))| d\mathbf{x} + \lambda \int_\Omega \int_\Omega H(\phi) K_\sigma(\mathbf{x} - \mathbf{y}) \\ &\quad \times \int_0^R |P_i(z) - P_r^{\mathbf{x}}(z)| dz d\mathbf{y} d\mathbf{x} + \lambda \int_\Omega \int_\Omega (1 \\ &\quad - H(\phi)) K_\sigma(\mathbf{x} - \mathbf{y}) \int_0^R |P_o(z) - P_r^{\mathbf{x}}(z)| dz d\mathbf{y} d\mathbf{x} \end{aligned} \quad (19)$$

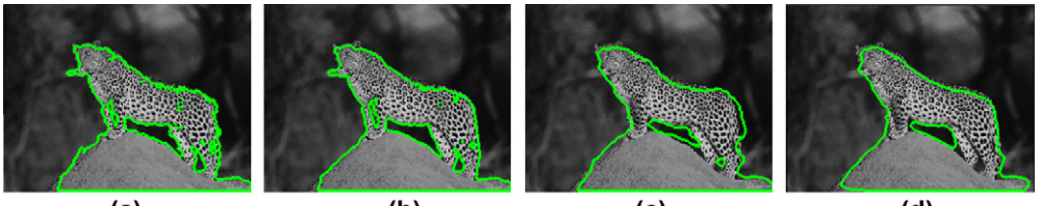

Fig. 1. Segmentation results using local histogram based ACM. The green curve in (a) and (c) are the segmentation results using L_1 distance with $r = 3$ and $r = 8$, respectively. The green curve in (b) and (d) are the segmentation results using Wasserstein distance with $r = 3$ and $r = 8$, respectively. (For interpretation of the references to color in this figure legend, the reader is referred to the web version of this article.)

For a fixed level set function ϕ, the energy functional $E(\phi, P_i^{\mathbf{x}}, P_o^{\mathbf{x}})$ with respect to $P_i^{\mathbf{x}}$ and $P_o^{\mathbf{x}}$ is minimized respectively. The updating functions of local fitting histograms can be obtained and are listed as follows:

$$P_i^{\mathbf{x}}(z) = \frac{\int_\Omega H(\phi) K_\sigma(\mathbf{x}-\mathbf{y}) P_r^{\mathbf{y}}(z) d\mathbf{y}}{\int_\Omega H(\phi) K_\sigma(\mathbf{x}-\mathbf{y}) d\mathbf{y}} \tag{20}$$

$$P_o^{\mathbf{x}}(z) = \frac{\int_\Omega (1-H(\phi)) K_\sigma(\mathbf{x}-\mathbf{y}) P_r^{\mathbf{y}}(z) d\mathbf{y}}{\int_\Omega (1-H(\phi)) K_\sigma(\mathbf{x}-\mathbf{y}) d\mathbf{y}} \tag{21}$$

Energy functional $E(\phi, P_i^{\mathbf{x}}, P_o^{\mathbf{x}})$ with $P_i^{\mathbf{x}}$ and $P_o^{\mathbf{x}}$ fixed is minimized with respect to ϕ. The gradient descent function of ϕ is as follows:

$$\frac{\partial \phi}{\partial t} = \delta(\phi) \cdot \left\{ \nabla \cdot \left(\frac{\nabla \phi}{|\nabla \phi|} \right) - \lambda \int_\Omega K_\sigma(\mathbf{x}-\mathbf{y}) \int_0^R (|P_i^{\mathbf{x}}(z) - P_r^{\mathbf{y}}(z)| - |P_o^{\mathbf{x}}(z) - P_r^{\mathbf{y}}(z)|) dz d\mathbf{y} \right\} \tag{22}$$

3.2. Varying the kernel width of the local fitting histogram

We introduce the local histogram fitting energy and make the model described in (10) has the ability of evolving the curve by local statistics using (19). Unfortunately, it brings in new problems summarized in Fig. 2. The green curve in Fig. 2(a) is the initialization, some part of which is placed outside the object. The yellow and red blocks ($\rho = 6$) in Fig. 2(b) are the statistical range for computing the local fitting histograms $P_i^{\mathbf{x}}(z)$ and $P_o^{\mathbf{x}}(z)$ by (20) and (21). One problem is that the local fitting histograms on each pixel of the red block inside and outside the evolving curve in Fig. 2 (b) are very similar, since the local histograms in this area are very similar. It leads to the value of evolution function (22) equal to 0. There is no curve evolution on this kind of points, see the evolving curve inside the leopard in Fig. 2(b)–(d). Another problem is that various parts of the evolving curve may evolve independently by computing their own local fitting histograms, such as the yellow and red block in Fig. 2(b). The yellow point on the green in Fig. 2(b) will evolve using its own local fitting histograms which are irrelevant to the real object.

The reason of the two problems in Eqs. (20)–(22) is lack of global region information. A solution is to increase the kernel width ρ. Disadvantage of the solution is that it extracts objects inaccurately. Fig. 3 shows the performances when larger kernel width is applied. The results in Fig. 3(a) and (b) suffer from the same problem of the result shown in Fig. 2(d). Fig. 3(c) and (d) show the results using more global statistics to compute the local fitting histogram, but they fail to discriminate the leopard from the mound. These experiments indicate that if a small ρ is applied, more fine results in real boundary will be obtained, but it creates too many local minima; if a larger ρ is applied, global information will be involved, but the curve will leak out from the real boundary as a result of lacking of the local information. Since none of the ρ applied in the experiments of Fig. 3 obtains a satisfactory result, the kernel width ρ of the local fitting histograms is argued to be varying during the curve evolution.

Our goal in this section is to use different kernel width ρ at different pixel to compute the local fitting histograms during curve evolution. The size of ρ is based on the similarity of the local fitting histograms inside and outside the evolving curve. If the two local fitting histograms are similar, which means that the local fitting histograms cannot correctly approximate the object and background, ρ should be increased; if the two local fitting histograms are very different, which means that the local fitting histograms can discriminate the object and background, ρ should not be changed. Three distances are defined to compare the similarity of the local fitting histograms of pixel $\mathbf{x}$ inside and outside the evolving curve. The three distances are defined as follows:

$$MinIn < \frac{D(P_{i,L}^{\mathbf{x}}, P_{i,C}^{\mathbf{x}})}{D(P_{i,L}^{\mathbf{x}}, P_{o,C}^{\mathbf{x}})} < MaxIn \tag{23}$$

$$MinOut < \frac{D(P_{o,L}^{\mathbf{x}}, P_{i,C}^{\mathbf{x}})}{D(P_{o,L}^{\mathbf{x}}, P_{o,C}^{\mathbf{x}})} < MaxOut \tag{24}$$

$$D(P_{o,C}^{\mathbf{x}}, P_{i,C}^{\mathbf{x}}) < \varepsilon \tag{25}$$

where $P_{i,L}^{\mathbf{x}}$, $P_{i,C}^{\mathbf{x}}$ are the local fitting histograms at position $\mathbf{x}$ computed by (20) inside the evolving curve using larger kernel width $\rho = L$ and current kernel width $\rho = C$ respectively. $P_{o,L}^{\mathbf{x}}$ and $P_{o,C}^{\mathbf{x}}$ are the local fitting histograms at position $\mathbf{x}$ computed by (21) outside the evolving curve using larger kernel width $\rho = L$ and current kernel width $\rho = C$ respectively. *MinIn*, *MaxIn*, *MinOut*, *MaxOut* and ε

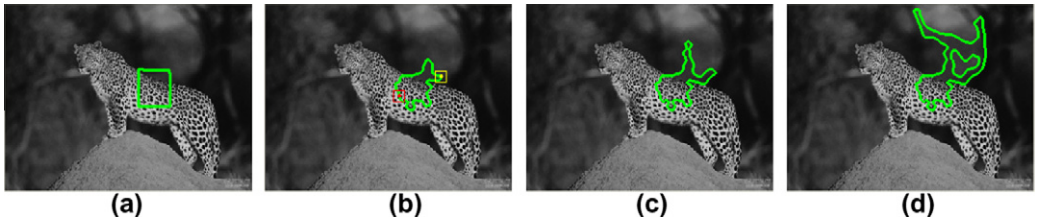

Fig. 2. Problems of active contour model using local histogram fitting energy: (a) initialization; (b, c) the evolution process; and (d) the final result. The kernal width in this experiment is set to $\rho = 6$.

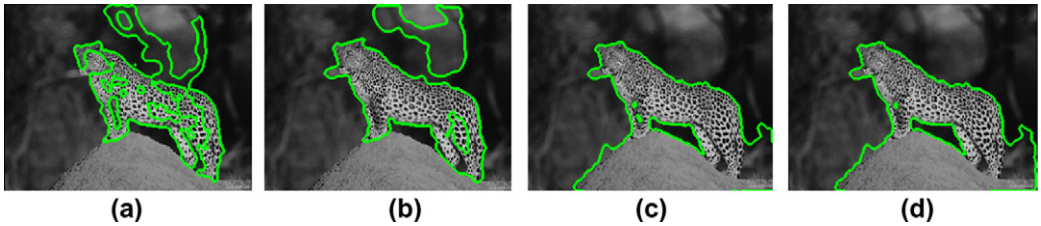

Fig. 3. Segmentation results using fixed ρ: (a–d) are the segmentation results using $\rho = 10$, $\rho = 20$, $\rho = 30$ and $\rho = 40$ respectively.

are predefined thresholds. Chi-2 distance (6) is utilized in the formula (23)–(25).

The inequality (23) and (24) are relative distances of the local fitting histograms of current kernel width. An absolute distance between $P^{\mathbf{x}}_{o,c}$ and $P^{\mathbf{x}}_{i,c}$ is defined in (25). Our method here is that a larger kernel width to compute the local fitting histograms and evolve the curve at $\mathbf{x}$ will be applied when any inequality in (23)–(25) is satisfied.

3.3. Implementation

The grey level of an image is often 256 (8-bit) or 4096 (12-bit). It is time consuming to compute the local histograms and the local fitting histograms using too rich grey level. Therefore original histogram is divided into B bins having an equal number of entries (Ojala et al., 2002). Then, a map is constructed for each image to be processed, which can map the bins from original grey level to the bins from new created grey level.

A fast two-cycle (FTC) level set method has been proposed (Shi and Karl, 2008) which report two orders of magnitude faster than the conventional one (Osher and Fedkiw, 2003). Integer-value sign function is applied to represent the evolving curve implicitly, which define that the value at all pixels outside the curve is 3, except at border pixels where the value is 1; the value at all pixels inside the curve is -3, except at border pixels where the value is -1. Thus, the evolving curve is described by bilateral linked lists that the values are -1 and 1. FTC divides the evolution speed F (usually $F = \partial\phi/\partial t$) by a data dependent speed $\hat{F}_d$ and a smoothness regularization speed $\hat{F}_{\text{int}}$ respectively. Sign of these speeds computed in the bilateral linked lists decide the direction of evolution. Since FTC utilize a Gaussian filter to smooth the evolving curve and keep the evolving curve regularized, the smoothness term $\nabla \cdot (\nabla\phi/|\nabla\phi|)$ in (22) is not needed for data dependent speed. Thus, the data dependent speed of our algorithm is defined by:

$$\hat{F}_d = -\int_{\Omega} K_\sigma(\mathbf{x}-\mathbf{y}) \int_0^R (|P^{\mathbf{x}}_i(z) - P^{\mathbf{y}}_r(z)| - |P^{\mathbf{x}}_o(z) - P^{\mathbf{y}}_r(z)|)dzd\mathbf{y} \quad (26)$$

The smoothness regularization speed $\hat{F}_{\text{int}}$ in our implementation is defined as same as that in FTC. $\hat{F}_d$ and $\hat{F}_{\text{int}}$ are used to evolve the curve alternatively, which will perform better when there are noise in the image.

For numerically computing the $\hat{F}_d$ of point $\mathbf{x}$ on the bilateral linked list via (26), a given kernel width ρ is required, for example $\rho = 6$. Then, σ can be obtained by $\sigma = \rho/2 = 3$ and the Gaussian mask can be computed via the method introduced in (Jain et al., 1995). For each pixel overlapped by the Gaussian mask, the local fitting histograms should be computed via (20) and (21) respectively, and then $\int_0^R (|P^{\mathbf{x}}_i(z) - P^{\mathbf{y}}_r(z)| - |P^{\mathbf{x}}_o(z) - P^{\mathbf{y}}_r(z)|)dz$ is computed via L_1 distance between local fitting histograms and local histogram of $\mathbf{x}$. These values are multiplied by the corresponding Gaussian mask value, and are added together to get the final $\hat{F}_d$.

Usually, L is set to 5C–10C. In particular, it can cover the whole image plane, namely $L = \infty$, then the local histogram fitting energy (18) will be the energy of the local histogram-based ACM in (10) and the local fitting histogram in (20) and (21) will be the global mean histogram defined in (14) and (15). Thus, local histogram-based ACM is a special case of our method.

The process of our algorithm can be summarized as follows

1. Reduce the original gray level of the image to be processed;
2. Select patch scale r, current kernel width C, larger kernel width L, thresholds $MinIn$, $MaxIn$, $MinOut$, $MaxOut$ and ε;
3. Initialize the evolving curve and compute the local histogram of each pixel;
4. Compute the local fitting histograms of the pixels in the bilateral linked list using current kernel width C;
5. Compute the local fitting histograms of the pixels in the bilateral linked list using larger kernel width L;
6. Check whether any of the inequality (23)–(25) is satisfied, if yes, using the larger kernel width and the corresponding local fitting histograms to evolve the curve (22) via FTC; if not, using the current kernel width and the corresponding local fitting histograms to evolve the curve (22) via FTC;
7. Check whether convergence or maximum number of iterations is reached. If not, go back to step 4.

4. Experimental results

Our algorithm is coded by C++. All of the experiments in this section are run in a release version of our code on an Intel Core 2 Quad Q8200 2.33 GHz CPU, 3.5 GB RAM computer. The bin number B and the patch scale r in the experiments of this section are set to 25 and 3, respectively.

The experiments in Fig. 4 show the evolution process from the initial curve (first column) to the final curve (fourth column) using local histogram fitting energy with varying kernel width. The first row of the experiments in Fig. 4 shows the segmentation results using $C = 6$ and $L = 30$. The parameters of inequality (23)–(25) are set as $MinIn = MinOut = 0.9$, $MaxOut = MaxIn = 1.1$ and $\varepsilon = 0.2$. The result in Fig. 4(d) is better than that in Figs. 1–3, since

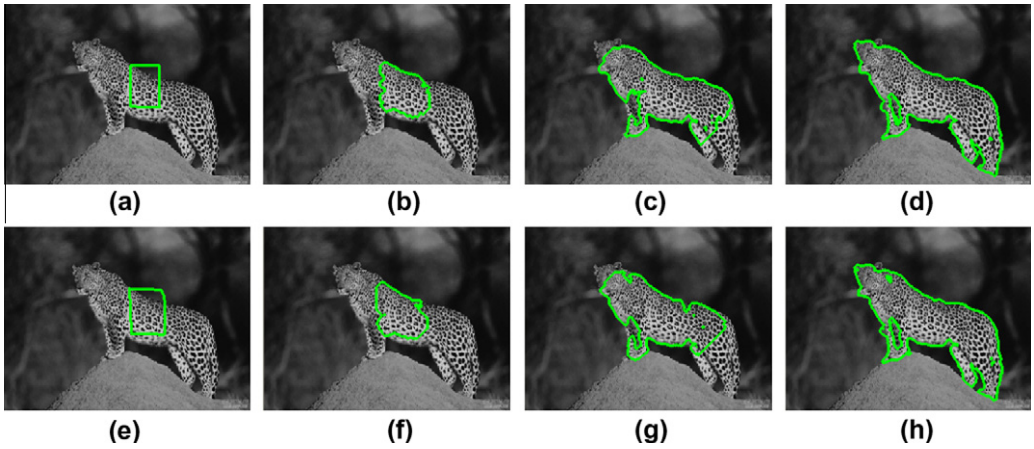

Fig. 4. Segmentation using varying kernel width: (a, e) the initialization; (b–d) the evolution process using $C = 6$ and $L = 30$; and (f–h) the evolution process using $C = 6$ and $L = \infty$.

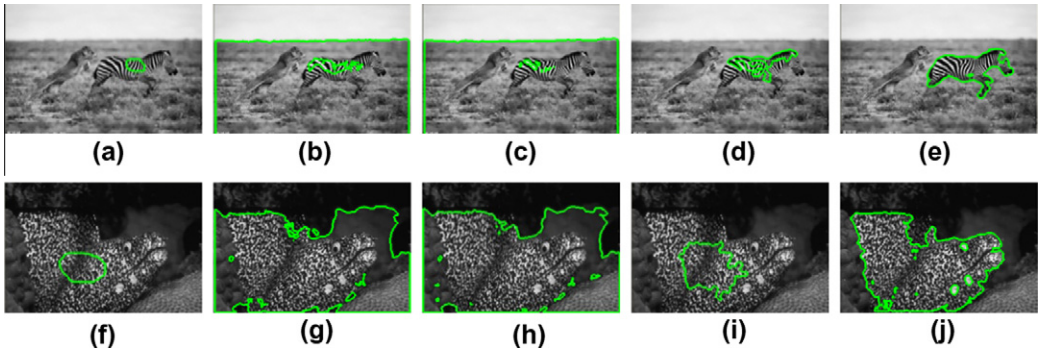

Fig. 5. Segmentation of natural texture images: the green closed contours in (a) and (f) are the initialization of the evolving curve; (b, g) the results of local histogram-based active contour model introduced in Section 2 using L_1 distance with 256 bins; (c, h) the results of local histogram-based active contour introduced in Section 2 using L_1 distance with 25 bins; (d, i) the results using Local histogram fitting energy with fixed kernel width presented in Section 3.1; and (e, j) the results using Local histogram fitting energy with varying kernel width presented in Section 3.2. (For interpretation of the references to color in this figure legend, the reader is referred to the web version of this article.)

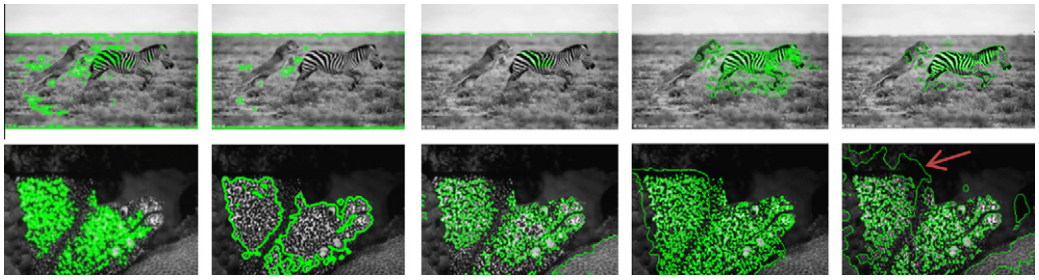

Fig. 6. Comparations of our method with other commonly used ACM. From left column to reight column are the segmentation results via the C–V model, the method presented by Ni et al. (2009), the method presented by Zhang et al. (2010b), LBF (Li et al., 2008), and LIF (Zhang et al., 2010a) respectively.

the local statistical feature and varying kernel width are applied. The second row of the experiments in Fig. 4 shows the segmentation results using $C = 6$ and $L = \infty$ that is a special case when the domain of larger kernel width covers the whole image plane. The parameters of inequality (23)–(25) are set as $MinIn = MinOut = 0.98$, $MaxOut = MaxIn = 1.02$ and $\varepsilon = 0.1$. The size of the leopard picture in this experiment is 268×202. The segmentation results in Fig. 4(d) and (h) are very similar, and the computation times are 38.14 s and 3.52 s, respectively.

The experiments in Fig. 5 show the improvement of our method step by step. When the image has a complex content, it is not appropriate to determine the curve evolution by comparing the distance between the local histogram and global mean histograms, see the results in Fig. 5(b), (c), (g) and (h). And there are not too many differences in this segmentation results when 256 or 25 bins are applied, which demonstrate that it is appropriate to reduce the number of histogram bins. The method using local histogram fitting energy introduced in Section 3.1 will be fall into the local minima in Fig. 5(d) and (i) when the initial curve is not initialized near the real boundary. Our methods perform well in Fig. 5(e) and (j) by varying the kernel width of the local fitting histograms. In this experiment, $C = 6$ and $L = \infty$. The parameters of the inequalities are set as $MinIn = MinOut = 0.98$, $MaxOut = MaxIn = 1.02$ and $\varepsilon = 0.1$. The sizes of the images in Fig. 5(a) and (f) are 300×200 and 300×200, and the computation times of our presented method in Fig. 5(e) and (j) are 3.35 s and 7.42 s, respectively.

A comparison of the accuracy in extracting the true boundary of the object is performed between our method and other five popular ACMs: the C–V model (Chan and Vese, 2001), the local histogram based ACM using Wasserstein distance (Ni et al., 2009), the ACM driven by region-based sign pressure force (Zhang et al., 2010b), the local binary fitting (LBF) energy model (Li et al., 2008) and the local image fitting energy model (Zhang et al., 2010a) in Fig. 6. The C–V model fails to segment the images, since it is hard to address the segmentation of nature texture image without texture feature analysis (Cao et al., 2008). The methods presented by Ni using Wasserstein distance which can faithfully measure the distance between two histograms by comparing bin to bin histogram measures. However, it is not appropriate to compare a local histogram of a pixel to the global mean histogram. The third column in Fig. 6 present the segmentation results via the method proposed in (Zhang et al., 2010b), which assumes the intensity inside and outside the evolving curve are homogeneous. In texture images, however, it is unwise to use the mean inside and outside the contour to represent the object and background. The results of LBF (Li et al., 2008) are shown in the fourth column of Fig. 6. LBF model which are proposed to address the intensity inhomogeneous problem via local fitting function. However, the kernel width of the local fitting function of the LBF is fixed. As we discussed in Section 3.2 and the experiments in Fig. 3, a same kernel width applied may cause local minima of the energy functional during the curve evolution. Different kernel widths are used to perform the experiment, but none of the results is satisfactory. The results of LIF (Zhang et al., 2010a) are shown in the final column of Fig. 6. LIF method also uses a fixed kernel width during the curve evolution, so it may be trapped by local minima. Moreover the evolution function of LIF method is defined as follows:

$$\frac{\partial \phi}{\partial t} = (I - I^{LFI})(m_1 - m_2)\delta(\phi)$$

where m_1 and m_2 are the local mean intensity of the background and object confined by a kernel width. I^{LFI} is the LFI proposed in (Zhang et al., 2010a). I is the intensity of the image. It is noticed that if $m_1 = m_2$ in the above equation, the curve will not evolve

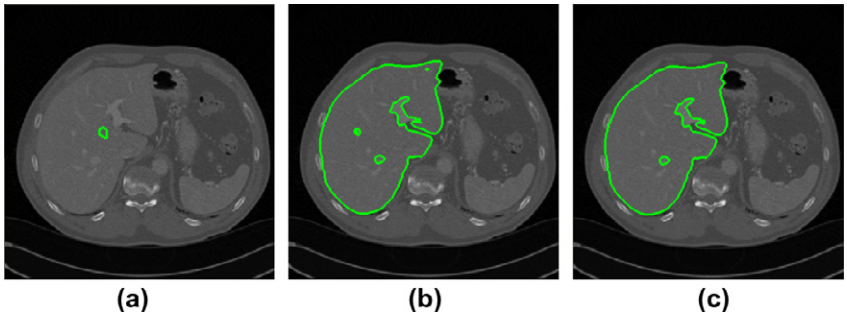

Fig. 7. Liver segmentation: (a) the initialization; (b) the segmentation results using $MinIn = MinOut = 0.99$, $MaxOut = MaxIn = 1.01$ and $\varepsilon = 0.05$; and (c) the segmentation results using $MinIn = MinOut = 0.98$, $MaxOut = MaxIn = 1.02$ and $\varepsilon = 0.1$.

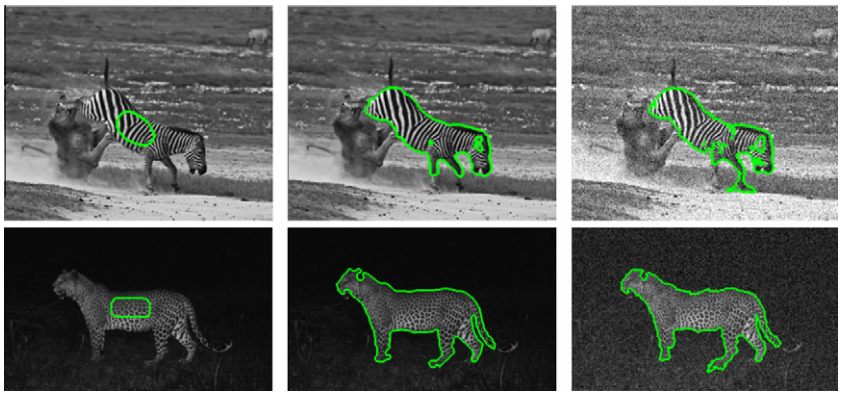

Fig. 8. Noise image segmentation. The parameters in this experiment are set by $MinIn = MinOut = 0.98$, $MaxOut = MaxIn = 1.02$, $\varepsilon = 0.1$, $C = 6$ and $L = \infty$.

anymore. Thus, the evolving curve will be trapped in some homogeneous region such as the contour pointed out by the red arrow in the last figure of Fig. 6.

Fig. 7 presents the results for liver segmentation in abdomen CT slicers. We use $C = 6$ and $L = \infty$ in this experiment. The curve is initialized by a small closed circle inside the liver in Fig. 5(a). The segmentation results are shown in (b) and (c) using different parameters. The results are very similar, except some vessel inside the liver will be missed when we apply a larger range of the inequalities.

Fig. 8 shows the segmentation results with and without Gaussian noise respectively. The first column shows the initialization of the active contour. The second column shows the segmentation results without noise disturbance. Gaussian noise of mean 25.5 and variance 25.5^2 is added to the image. The segmentation results of these noise polluted images are shown in the third column of Fig. 8. The noise will disturb the computation of the local histograms. Without tuning the parameters of the inequalities (23)–(25), our method can give similar results to the unpolluted images. We therefore drew a conclusion that the noise influences all of the histograms equally.

5. Conclusion

In this paper, a nonparametric local region-based active contour model in level set framework is presented. Our method applies the nonparametric statistic and does not predefine any kind of distribution of each region. It is not appropriate to use a fixed kernel width when compute the local fitting histograms and evolve the curve. A method for varying the kernel with is presented in this study. Three inequality equations are defined. If any of the one is satisfied, a larger kernel width is encouraged. The bin number is reduced and fast level set method is used to improve the computational speed. The experimental results demonstrate that the proposed method is able to segment texture images and low contrast image.

Acknowledgements

This paper was supported by the National Basic Research Program of China (No. 2010CB732506) and National Science and Technology Support Projects of China (No. 2012BAH07B01).

References

Broadhurst, Robert E., Stough, Joshua, Pizer, Stephen M., Chaney, Edward L., 2006. A statistical appearance model based on intensity quantile histograms. In: IEEE Internat. Symposium on Biomedical Imaging, pp. 422–425.

Cao, Guo, Mao, Zhihong, Yang, Xin, Xia, Deshen, 2008. Optical aerial image partitioning using level sets based on modified Chan–Vese model. Pattern Recognition Lett. 29, 457–464.

Caselles, Vicent, Kimmel, Ron, Sapiro, Guillermo, 1997. Geodesic active contours. Internat. J. Comput. Vision 22, 61–79.

Chakraborty, Amit, Staib, Lawrence H., Duncan, James S., 1996. Deformable boundary finding in medical images by integrating gradient and region information. IEEE Trans. Med. Imaging 15, 859–870.

Chan, Tony F., Vese, Luminita A., 2001. Active contours without edges. IEEE Trans. Image Process. 10, 266–277.

Chan, Tony, Esedoglu, Selim, Ni, Kangyu, 2007. Histogram based segmentation using Wasserstein distance. In: Proc. Scale Space and Variational Methods in Computer Vision, pp. 697–708.

Chen, Siqi, Radke, Richard J., 2009. Level set segmentation with both shape and intensity priors. In: IEEE Internat. Conf. on Computer Vision, Kyoto, pp. 763–770.

Freedman, Daniel, Zhang, Tao, 2004. Active contours for tracking distributions. IEEE Trans. Image Process. 13, 518–526.

Freedman, Daniel, Radke, Richard J., Zhang, Tao, Jeong, Yongwon, Lovelock, Michael, Chen, George T.Y., 2005. Model-based segmentation of medical imagery by matching distribution. IEEE Trans. Med. Imag. 24, 281–292.

Hong, Byung-Woo, Soatta, Stefano, Ni, Kangyu, Chan, Tony, 2008. The scale of a texture and its application to segmentation. In: IEEE Conf. on Computer Vision and Pattern Recognition, Anchorage, AK, pp. 1–8.

Jain, Ramesh, Kasturi, Rangachar, Schunck, Brain G., 1995. Machine Vision. McGraw-Hill, Beijing.

Jehan-Besson, Stephanie, Barlaud, Michel, Aubert, Gilles, 2003. Shape gradients for histogram segmentation using active contours. In: IEEE Internat. Conf. on Computer Vision, Nice, France pp. 408–415.

Kass, Michael, Witkin, Andrew, Terzopoulos, Demetri, 1988. Snakes: Active contour models. Internat. J. Comput. Vision 1, 321–331.

Kim, Junmo, Fisher, John W., Yezzi, Anthony, Cetin, Mujdat, Willsky, Alan S., 2005. A nonparametric statistical method for image segmentation using information theory and curve evolution. IEEE Trans. Image Process. 14, 1486–1502.

Lankton, Shawn, Tannenbaum, Allen, 2008. Localizing region-based active contours. IEEE Trans. Image Process. 17, 2029–2039.

Li, Chunming, Kao, Chiu-Yen, Gore, John C., Ding, Zhaohua, 2008. Minimization of region-scalable fitting energy for image segmentation. IEEE Trans. Image Process. 17, 1940–1949.

Luo, Zhonghua, Wu, Jitao, 2011. The integration of directional information and local region information for accurate image segmentation. Pattern Recognition Lett. 32, 1990–1997.

Ma, Yu, Xiaodong, Gu, Wang, Yuanyuan, 2010. Histogram similarity measure using variable bin size distance. Computer Vision and Image Understanding 114, 981–989.

Melonakos, John, Pichon, Eric, Angenent, Sigurd, Tannenbaum, Allen, 2008. Finsler active contours. IEEE Trans. Pattern Anal. Machine Intell. 30, 412–423.

Ni, Kangyu, Bresson, Xavier, Chan, Tony, Esedoglu, Selim, 2009. Local histogram based segmentation using the Wasserstein distance. Internat. J. Comput. Vision 84, 97–111.

Ojala, Timo, Pietikainen, Matti, Maenpaa, Topi, 2002. Multiresolution grey-scale and rotation invariant texture classification with local binary patterns. IEEE Trans. Pattern Anal. Machine Intell. 24, 971–987.

Osher, Stanley, Fedkiw, Ronald, 2003. Level Set Methods and Dynamic Implicit Surfaces. Springer, New York.

Paragios, Nikos, Deriche, Rachid, 2002. Geodesic active regions and level set methods for supervised texture segmentation. Internat. J. Comput. Vision 46, 223–247.

Paragios, Nikos, Mellina-Gottardo, Olivier, Ramesh, Visvanathan., 2004. Gradient vector flow fast geometric active contours. IEEE Trans. Pattern Anal. Machine Intell. 26, 402–407.

Piovano, Jérome, Papadopoulo, Théodore, 2008. Local statistic based region segmentation with automatic scale selection. In: Proc. European Conf. on Computer Vision, pp. 486–499.

Rousson, Mikael, Deriche, Rachid, 2002. A variational framework for active and adaptative segmentation of vector valued images. In: IEEE Workshop on Motion and Video Computing, Orlando, Florida, pp. 56–62.

Shang, Yangfeng, Yang, Xin, Zhu, Lei, Deklerck, Rudi, Nyssen, Edgard, 2008. Region competition based active contour for medical object extraction. Comput. Med. Imaging Graphics 32, 109–117.

Shang, Yangfeng, Markova, Aneta, Deklerck, Rudi, Nyssen, Edgard, Yang, Xin, de Mey, Hohan, 2010. Liver segmentation by an active contour model with embedded Gaussian mixture model based classifiers. In: Proc. SPIE Optics, Photonics, and Digital Technologies for Multimedia Applications, Brussels, Belgium, p. 772313.

Shi, Yonggang, Karl, William Clem, 2008. A real-time algorithm for the approximation of level-set-based curve evolution. IEEE Trans. Image Process. 17, 645–656.

Tsai, Andy, Yezzi, Anthony, Willsky, Alan S., 2001. Curve evolution implementation of the Mumford–Shah functional for image segmentation, denoising, interpolation, and magnification. IEEE Trans. Image Process. 10, 1169–1186.

Vese, Luminita A., Chan, Tony F., 2002. A multiphase level set framework for image segmentation using the Mumford and Shah model. Internat. J. Comput. Vision 50, 271–293.

Wang, Li, He, Lei, Mishra, Arabinda, Li, Chunming, 2009. Active contours driven by local Gaussian distribution fitting energy. Signal Process. 89, 2435–2447.

Xie, Xianghua, Mirmehdi, Majid, 2004. RAGS: Region-aided geometric snake. IEEE Trans. Image Process. 13, 640–652.

Xie, Xianghua, Mirmehdi, Majid, 2008. MAC: Magnetostatic active contour model. IEEE Trans. Pattern Anal. Machine Intell. 30, 632–646.

Zhang, Kaihua, Song, Huihui, Zhang, Lei, 2010a. Active contours driven by local image fitting energy. Pattern Recognition 43, 1199–1206.

Zhang, Kaihua, Zhang, Lei, Song, Huihui, Zhou, Wengang, 2010b. Active contours with selective local or global segmentation: A new formulation and level set method. Image Vsion Comput. 28, 668–676.